Electronic Journal of Structural Engineering

Original Article

Cite this: DOI:10.56748/ejse.26835

Received Date: 3 June 2025
Accepted Date: 28 November 2025

1443-9255
https://ejsei.com/ejse

Buckling of Multi-Span Frames with Newmark Method

Ashraf Badir [a*]

[a] Department of Bioengineering, Civil Engineering and Environmental Engineering U.A. Whitaker College of Engineering, Florida Gulf Coast University, Fort Myers, FL 33965, USA
*Corresponding author: abadir@fgcu.edu

Abstract

Newmark's numerical method of computing deflections, moments and buckling loads of isolated columns is extended for the analysis of elastic buckling loads and buckling modes of prismatic and non-prismatic single story, multi-span frames with combinations of hinged and fixed columns. Step-by-step description of the developed procedure is presented, using statics equilibrium, slope deflection equations and boundary conditions. The elastic line of the buckling mode is determined as a major part of the solution, and the numerical procedure is used to calculate the buckling loads and the columns' effective length factor for multi-span frames. The most favorable variation of cross-section of tapered frame columns is calculated, giving the maximum possible elastic critical load of the frame for constant columns' volume.

Keywords

Newmark method, Buckling loads, Stability, Effective length, Sway frames, non-prismatic columns

1. Introduction

Structures are commonly designed to achieve both economic and safety goals. For ordinary structures, economy frequently imposes the selection of standard steel sections or regular reinforced concrete shapes. However, for other structures, such as more complicated, unique, or large ones, using non-prismatic or tapered members may enhance structural efficiency and reduce overall cost.

Studies in column buckling go back to the eighteenth century, with the experimental work of Musschenbroek (1729), constituting apparently the first study in the literature on column buckling (Godoy and Elishakoff, 2020), and the mathematical work of Euler (1778). In the Nineteenth century, accelerated metal construction raised interest in buckling investigations, and the study of elastic stability continued with the twentieth century classical work of Timoshenko and Gere (1964), among others.

Although numerical or approximate methods, such as the finite element method and the finite difference method play an important role in the solution of stability problems, the effective length method has been widely used for stability evaluation and design of compression members for many years. Columns are considered in isolation with end restraints, and the effective length factor is evaluated based on the joint stiffness ratio at each end of the column (Julian and Lawrence, 1959). This procedure is currently adopted by the American Concrete Institute, ACI 318 (2025) and the American Institute of Steel Construction, AISC (2023). Efforts have been made to improve the accuracy of the method and extend its range of validity by considering the difference in the boundary conditions of top and bottom columns by Duan and Chen (1988, 1989, 1999) and Kishi et al. (1997), among others.

The non-contradictory complementary information (NCCI) document SN008a (Oppe et al., 2005) to BS EN 1993-1 (BSI, 2005) rely on the effective length method to assess the stability of multi-story frames and provides erroneous results in certain situations (Webber et al 2015) because it omits the contribution made to the rotational stiffness of the end restraints by columns above and below, and to the translational stiffness of end restraints by other columns in the same story.

Many studies have been conducted on the design of columns with variable cross-section in single-span gable frames. A mathematical analytical method was presented for determining the effective length factor for non-prismatic columns in two-span gable frames (Behjati-Avval and Vahidreza, 2015). A formulation of the stability of non-prismatic frames with flexible connections and elastic supports (Rezaiee-Pajand et al. 2016) was presented based on the solutions of the governing differential equations for buckling. Studies aimed at the interaction effect among sway-permitted stepped columns to develop a practical approach to consider this effect have been presented by Tian et al (2021a, b). These studies were based on the slope-deflection method and the concept of story-based buckling.

In a comprehensive historical review, Pomares et al. (2021) examined the evolution of buckling models used in the design of steel structures over the past 275 years. Their study highlighted the limitations of traditional analytical methods and emphasized the need for improved accuracy in predicting buckling behavior, especially in light of catastrophic failures such as the Dee Bridge, 1847, Tay Bridge, 1879, Quebec Bridge, 1907, and Tacoma Bridge, 1940. By comparing historical models with finite element simulations of compressed steel columns, the authors demonstrated significant discrepancies in safety predictions and advocated for the integration of modern computational techniques to enhance structural reliability.

Buckling and stability analysis of structural frames has long been a central concern in structural engineering. The classical theory of buckling began with Euler's formulation for slender columns, which laid the foundation for understanding critical load behavior under axial compression. Over time, this theory was extended to more complex systems such as plates, shells, and multi-member frames.

In frame structures, buckling can occur in two primary modes: column buckling of individual members and global frame buckling, where the entire frame undergoes lateral displacement. These modes are influenced by member stiffness, joint rigidity, and load eccentricities. Traditional design approaches, such as the effective length method and P-Δ analysis, have been widely used to estimate buckling loads. However, these methods often rely on simplifications that may not capture the true behavior of complex frames under combined loading conditions (Schilling, 1983). Recent developments have emphasized the importance of second-order effects and the interaction between vertical and lateral loads. Schilling (1983) proposed a conservative method for estimating frame buckling loads using first-order analysis, incorporating correction factors for P-Δ effects.

The literature on frame buckling has evolved from simplified hand calculations to sophisticated computational models. The finite element method (FEM) has become a powerful tool for analyzing buckling in advanced materials and structural systems. Recent studies have focused on functionally graded materials (FGMs), carbon nanotube-reinforced composites (CNTRCs), and porous structures, which offer enhanced mechanical properties and design flexibility. Tati (2021) developed a four-node FEM model based on high-order shear deformation theory to analyze thermal and mechanical buckling of functionally graded (FG) plates. The model avoids shear locking and does not require correction factors, making it efficient and accurate for complex loading scenarios. Rayhan et al. (2025) combined FEM with machine learning to predict buckling strength in additively manufactured lattice stiffened panels. Their study demonstrated that simple cubic lattice structures outperform other configurations in buckling resistance, and polynomial regression models can accurately predict critical loads. Belabed et al. (2024) contributed extensively to FEM-based analysis of FG-CNTRC beams and plates, addressing free and forced vibration, elastic stability, and the effects of porosity and foundation types. Their quasi-3D and p-version FEM models have been validated against experimental and analytical benchmarks.

Tounsi et al. (2024) and Lakhdar et al. (2024) explored the dynamic behavior of porous FG nanocomposite beams and shells using advanced FEM formulations, including third-order shear deformation theory and viscoelastic foundation modeling.

Bentrar et al. (2023) and Katiyar et al. (2022) investigated the influence of porosity distribution and geometric imperfections on buckling and vibration behavior in FG sandwich plates and bi-directional FG plates, respectively, using FEM.

These studies collectively highlight the versatility of FEM in capturing the complex interactions between geometry, material gradation, and loading conditions. The integration of machine learning further enhances predictive capabilities, offering new avenues for design optimization and real-time structural assessment.

An optimization of no sway plane rigid frames against buckling centered on either maximizing the buckling load or minimizing the weight of the structures, or both was presented by Naidoo and Li (2019), it proved successful for no-sway multi-story rigid frames. An improved method for simplified frame stability analysis that accounts for the vertical interaction effects of columns was presented by Li et al. (2016). The governing equation for the elastic buckling load of the sub-assemblage is derived. The method is applicable to both sway-permitted and sway-prevented frames. The applicability and accuracy of the method were demonstrated using a series of examples with a wide variation of parameters including numbers of story, boundary conditions, stiffness of beam-to-column connections, column length and stiffness, and axial force level.

Buckling of tapered heavy columns with constant volume under self-weight and tip load has been recently presented by Lee and Lee (2021). The differential equation governing the buckling shapes of the column was derived based on the equilibrium equations of the buckled column elements. A new approach of the buckling analysis of non-prismatic columns was proposed by Nikolić and Šalinić (2017), using a rigid element method. An approximate computation of buckling loads for plane steel frames with tapered members was proposed by Bazeos and Karabalis (2006). The method was based on a series of dimensionless charts which have been developed using the exact solution of the Bernoulli-Euler beam theory and a wide range of steel profiles.

The critical elastic buckling load of an isolated bar with uniform or non-uniform cross section can be calculated by Newmark's (1943) numerical method of double integration. When the bar has a cross section varying along the span, a numerical procedure of successive approximation is useful. Instead of assuming deflection y as some function of x, the bar is divided into segments, and a numerical value of deflection is assumed for each division point, or station along the beam. The subsequent calculations are made in tabular form, calculating ordinates of the elastic load and deflections at each station. Comparing the final deflections with the initially assumed values determines the critical load. Bradford and Yazdi developed an analytical procedure based on the Newmark method, applicable to struts with geometric and material nonlinearities (1999). The Newmark method has been extended for use in computing buckling loads and buckling modes of single span elastic frames with either hinged or fixed columns, but not both (Badir 2011, 2020).

In this study, a numerical procedure to calculate critical loads and buckling modes for rigidly joined elastic multi-span sway portal frames with combination of hinged and fixed columns is presented. The single-story frames studied in this paper consist of sway frames having prismatic and non-prismatic columns, hinged or fixed directly into the foundation. The frames have a constant height with variable beam spans as shown in Fig. 1.

The developed method is applicable to the design and analysis of steel and reinforced concrete frames in buildings, bridges, and industrial structures. It is particularly beneficial in the following scenarios: design of frames with tapered columns for optimal buckling resistance, irregular non-prismatic column geometries, evaluation of effective length factors in multi-span systems with mixed boundary conditions, retrofitting and strengthening of existing frames where accurate buckling analysis is essential, and Optimization of material usage by maximizing critical loads under volume constraints. These applications demonstrate the method's relevance to real-world engineering problems.

The accurate prediction of elastic buckling loads and modes in multi-span frames is a critical aspect of structural stability analysis. Many structural systems, such as building frames, bridge piers, and industrial structures are composed of multiple spans with varying support conditions. Traditional buckling analysis methods often focus on isolated columns or simplified frame configurations, which may not capture the true behavior of complex systems. By extending Newmark's numerical method to multi-span frames, this research provides a more comprehensive and adaptable tool for engineers to assess buckling behavior, leading to safer and more efficient structural designs. Older methods like Newmark's method offer transparent, step-by-step procedures that help engineers and students understand the mechanics of buckling. Extending such methods preserves their pedagogical value while adapting them to more complex systems. While finite element methods provide powerful computational tools, they often obscure the underlying mechanics. The extended Newmark method retains analytical transparency, making it suitable for educational and preliminary design purposes. Moreover, it preserves historical continuity in the structural analysis field.

The research presented herein extends Newmark's numerical technique originally developed for isolated columns to multi-span frames with both prismatic and non-prismatic members. Detailed description of the developed numerical procedure is outlined, and sample examples are provided to illustrate the efficiency of the method. The method combines static equilibrium, slope-deflection equations, and boundary conditions to compute buckling loads, buckling mode shapes, and effective length factors in a unified approach. The procedure is introduced and used to determine the most favorable variation of column cross-section (tapering) that maximizes the elastic critical load for a given volume. The ratio between the depths of the top and bottom tapered rectangular columns yielding the maximum possible critical load of the frame is determined. These contributions advance the state of the art in buckling analysis and provide engineers with a powerful tool for structural optimization of irregular column shapes.

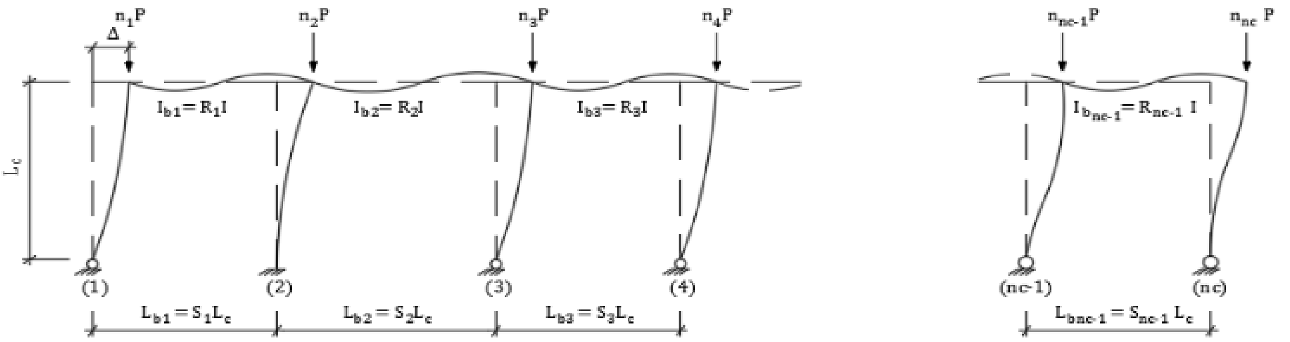

Fig. 1 Sway buckling mode of multi-span frames.

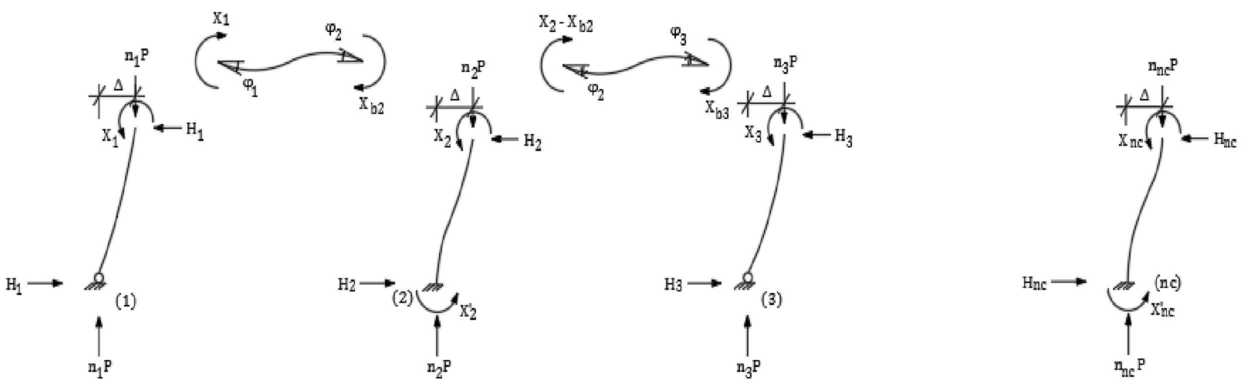

Fig. 2 Sway buckling mode of multi-span frames: end forces and rotations.

2. Method - Sway buckling modes of multi-span frames

The multi-span frame shown in Fig. 1 has a number of columns equal to *nc*. The frame is subjected to vertical concentrated loads at the top of the *nc* columns equal to *P* multiplied by a factor varying from n_1 to n_{nc} from left to right. The height of the columns is equal to L_c. The frame has (*nc*-1) spans with varying lengths from S_1L_c to $S_{nc-1}L_c$. The moment of inertia of the rafts is denoted by $I_{bi} = R_i I$ in which *i* varies from 1 to (*nc*-1).

The forces acting on each column are separately shown in Fig. 2 with a subscript number referring to the column by order from left to right.

The relations between the different unknowns are obtained from the following conditions:

2.1 Statics equations

$n_1P\Delta - X_1 - H_1L_c = 0$
$n_2P\Delta - X_2 - H_2L_c - X_2' = 0$
$n_3P\Delta - X_3 - H_3L_c = 0$
…………………………..
…………………………..
$n_{nc}P\Delta - X_{nc} - H_{nc}L_c - X_{nc}' = 0$ (1)

By superposition of Eq (1), and noticing that $\sum_{i=1}^{i=nc} H_i = 0$, then
$P\Delta \sum_{i=1}^{i=nc} n_i = \sum_{i=1}^{i=nc}(X_i + X_i')$ (2)
Where X_i' is the moment at the bottom fixed support, for hinged columns, X_i' are equal to zero.

2.2 Slope deflection equations

The relations between the end moments, at the top of each column (X_1, X_2, X_3,…, X_{nc}) and the angle of rotation of each joint (φ_1, φ_2, φ_3,…, φ_{nc}) can be obtained by studying each horizontal beam taking into consideration that $X_2 = X_{b2} + (X_2 - X_{b2})$, $X_3 = X_{b3} + (X_3 - X_{b3})$ and so on. Thus, neglecting the effect of axial forces in the horizontal beams, for *i = 1 to nc*, we obtain the *nc* slope deflection equations

$X_i = 2k_{bi-1}\varphi_{i-1} + 4(k_{bi-1} + k_{bi})\varphi_i + 2k_{bi}\varphi_{i+1}$ (3)

where X_i = end moment of column number *i*, $K_{bi} = EI_{bi}/L_{bi} = ER_iI/S_iLc$, φ_i = angle of rotation of joint number *i*. Noting that for *i* = 1, $K_{bi-1} = K_{bo} = 0$ and for *i = nc*, $K_{bi} = K_{bnc} = 0$.

2.3 Boundary conditions

From the condition of equal sway value Δ at the top of each column and from studying each fixed column separately, a set of equations is obtained. These equations together with static and slope deflection equations are sufficient to evaluate the unknowns X, H, and φ for all the columns, as described in detail in the following procedure:

1. Assume elastic line y_a for each column.
2. Start by assuming equal end moments (X_i) at the top of each column, and $X_i' = 0.5X_i$ at the bottom of each fixed column. Hence initial values of X_i and X'_i are obtained from Eq. (2).
3. From Eq. (1) the values of the horizontal forces (H_i) are calculated.
4. Find internal bending moments for each column. Hinged columns are subjected to the three previously suggested forces obtained from steps 2 and 3. Fixed columns are considered by the superposition of the three cases shown in Fig. 3.
5. Find elastic lines, with zero slope at column bottom for fixed columns, and zero slope at column top for hinged columns (will be corrected). This step will yield to the determination of a trial deflection at the top of each hinged column y_t, a correction value yc must be added to y_t.
6. The unknown forces and rotations, namely *X*, *H* and φ at the top of each column, with a total number of 3*nc*, are obtained from static equilibrium equations, slope deflections equations and boundary conditions.

The number of equations of static equilibrium equals (1 + nc_h), where nc_h is the number of hinged columns. These equations are $\sum H = 0$ plus only hinged column equations selected from Eq**Error! Reference source not found.** (1). The number of slope deflection equations = *nc*, given by Eq (3). The boundary conditions are determined from the slope and sway equations; providing (nc_f + *nc* - 1) equations, as shown below, in which nc_f is the number of fixed columns. These boundary conditions are now discussed in detail.

The slope at the top of each fixed column, Fig. 3, is
$\varphi_i = \varphi_{n_ip} + X_i\varphi_{X_i=1} + H_i\varphi_{H_i=1}$ (4)
with a total of nc_f equations. The value of the sway at the top of each column is $y_i = y_{n_ip} + X_iy_{X_i=1} + H_iy_{H_i=1}$ for fixed columns as shown in Fig. 3, and $y_i = y_{it} + \varphi_iL_c$ for hinged columns, where φ_iL_c is the top column sway correction. These values are all equal to the sway value Δ, therefore, for fixed columns
$y_{n_ip} + X_iy_{X_i=1} + H_iy_{H_i=1} = \Delta$ (5)
and for hinged columns
$y_{it} + \varphi_iL_c = \Delta$ (6)
Eqs. (5) and (6) constitute (*nc* – 1) equations, together with Eq (4) provide a total of (nc_f + *nc*-1) boundary condition equations. Thus, from static, slope deflection and boundary equations, a total number of 3*nc* equations are deduced and the 3*nc* unknowns (*X*, *H* and φ at top of each column) are determined.

7. From Eq. (1) find new X'_i.
8. Find resulting deflections *y* for each column. For hinged columns the resulting deflection is obtained by adding the trial deflection y_{it} to the linear correction value, varying from zero at the bottom hinge to $y_{ic} = \varphi_iL_c$ at the top of the column.
9. Repeat the cycle using *y* from step 8 as y_a of step 1 in the subsequent cycle.

The philosophy of the described method can be summarized as follows: the buckling load of the structure is the load just enough to maintain it in an assumed buckling configuration, provided that this load will in turn produce the assumed configuration. The method involves cycles of iteration in which a new configuration is obtained better than the assumed one at the end of each cycle. The calculations can be repeated until the required degree of accuracy is obtained.

3. Numerical Results

The versatility of the presented analysis can be demonstrated in dealing with stability problems of frames having non-prismatic column members, which are often encountered in both concrete and steel structures. Consider the anti-symmetrical mode of buckling of the frame shown in Fig. 4, with three spans. The span lengths are L_1 = 5.0 m, L_2 = 6.0 m, and L_3= L_1 = 5.0 m; where L_1, L_2 and L_3 are the distances between *AD, DD'* and *D'A'*, respectively.

Each column is divided into six segments with equal lengths, and the moments of inertia of all the columns vary as illustrated at each section for column AB (not shown for the other three columns). A numerical value of deflection is assumed for each division point, or station along the column. An arbitrary sidesway value of Δ = 1000 units is chosen. Using Eq. (2), and following the notation given in Fig. 2, considering $X_1 = X_4$ and $X_2 = X_3$ due to anti-symmetry, we obtain
$X_1 + X_2 = 2.56P\Delta = 2560P$ (7)
It has been deduced from solving many cases that it is good practice to begin with an equal value of the moments at the top of all the columns. Thus $X_1 = X_2$= 1280P are suggested values for the first cycle. These initial values will be altered from cycle to cycle until they reach their correct values. Fig. 5 shows complete calculations of the last cycle, in which both columns AB and DC are subjected to the different forces reached at this cycle. Each column is divided into 7 sections (6 segments of equal length λ, where λ = L_c/6). Details of each step are as follows:

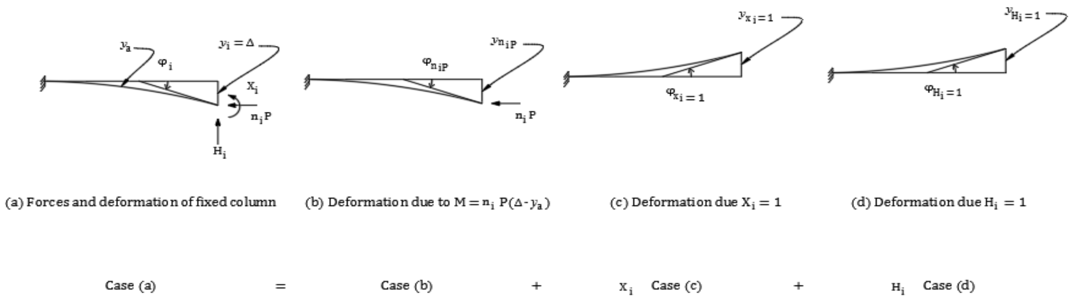

Fig. 3 Deformation superposition of fixed columns

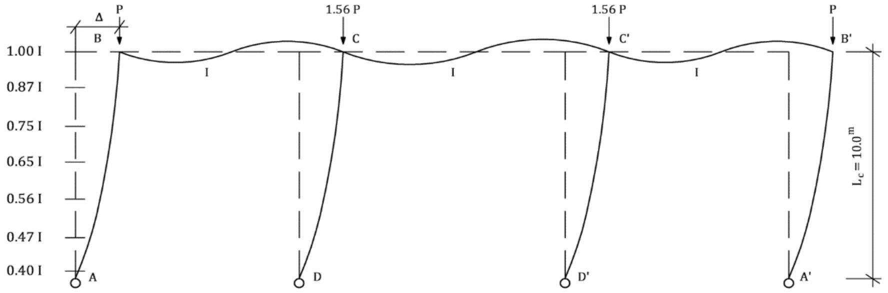

Fig. 4 Frame with non-prismatic columns

Line 1: assumed buckling mode obtained from previous cycle (a comment on the first cycle is given at the end of the detailed steps and shown in Table 1). The suffixes 1 and 2 correspond to columns AB and DC, respectively.

Line 2: moments in each column. A common factor is shown at the end of each line, for line 2 the common factor is P.

Line 3: flexural rigidity EI_c for both columns AB and DC.

Line 4: angle changes α ($\alpha = M/ EI_c$), commonly known as the elastic load.

Line 5: equivalent concentrated elastic loads $\bar{\alpha}$ acting on each section. The values of these concentrations are computed with sufficient accuracy from the formulae given in the work of Newmark (1943).

Line 6: assumed average slopes φ_{av} beginning with zero slope at the column ends B and C (will be corrected).

Line 7: trial deflections (y_{1t} and y_{2t}) based on the assumed average slopes and beginning with zero deflections at A and D.

Line 8: correction deflections y_{1c} and y_{2c} for column AB and DC, respectively. These corrections are linear beginning from zero at A and D to certain values at B and C. These values are obtained from the following relations:

(a) true slope = assumed slope + slope correction; hence, at B, B, $\varphi_1 = 0 + \varphi_{1c}$ and at C, $\varphi_2 = 0 + \varphi_{2c}$. From slope deflection equations, $X_1 = (EI/L_1)(4\varphi_1 + 2\varphi_2)$, $X_3 = (EI/L_1)(2\varphi_1 + 4\varphi_2)$ and $X_2 - X_3 = (EI/1.2L_1)6\varphi_2$. By superposition we get $X_1 + X_2 = (EI/L_1)(6\varphi_1 + 11\varphi_2)$. Noticing that $L_1 = 0.5L_c = 3\lambda$and $(X_1 + X_2) = 2560P$ from Eq. (7), then

$$2560P = \frac{EI}{3\lambda}(6\varphi_1 + 11\varphi_2) \quad (8)$$

(b) True deflection y1 at B, $y_{1t} + y_{1c}$ = true deflection y_2 at C, $y_{2t} + y_{2c}$. Since $y_{1c} = 6\varphi_{1c}\lambda = 6\varphi_1\lambda$, and $y_{2c} = 6\varphi_{2c}\lambda = 6\varphi_2\lambda$, therefore,

$$\underbrace{y_{1t}}_{\text{at B}} + 6\varphi_1\lambda = \underbrace{y_{2t}}_{\text{at C}} + 6\varphi_2\lambda \quad (9)$$

From line 7 Fig. 5, y_{1t} at B = 22361 $P\lambda^2$/EI and y_{2t} at C = 25811 $P\lambda^2$/EI. By solving Eqs. (8) and (9) we get $\varphi_1 = 823.83P\lambda/EI$ and $\varphi_2 = 284.83P\lambda/EI$. Thus $y_{1c} = 4943P\lambda^2/EI$ and $y_{2c} = 1493P\lambda^2/EI$. Based on the correction values of the deflections at B and C ($4943P\lambda^2/EI$ and $y_{2c} = 1493P\lambda^2/EI$), the linear corrections of columns AB and DC are entered in line 8.

Line 9: line 7 + line 8. This line gives true deflections y_1 and y_2.

Line 10: line 1/line 9. It gives ratios of the assumed and resulting deflections which are almost identical at all division points.

The better ratio $\Sigma y_a/\Sigma y$ is 0.03662 $EI/P\lambda^2$. Equating this ratio to unity, the value of the critical load is 1.3182 EI/L_c^2 and the effective length factor k of the hinged column AB is equal to 2.736; where $P_{cr} = \pi^2 EI/(kL_c)^2$ The same problem was solved analytically by deriving the slope-deflection equations for beam-columns made of solid bars, whose cross-sections varies as pyramids or truncated cone (Krynicki and Mazurkiewicz 1964) and a value of 1.31 EI/L_c^2 was obtained.

The suggested starting buckling mode of the subsequent cycle (last two lines of Fig. 5) is almost identical to the previous one, thus the shape of the columns at the critical condition is already obtained with a high degree of accuracy.

The previous problem was solved five times, beginning with five different assumed sets of deflection (ya) as shown in Table 1. In all cases, both the same critical load and the true buckling mode were reached. Special attention must be given to the last case where different shapes are assumed for each column of the frame, an assumption quite unreasonable, nevertheless the true anti-symmetrical mode of buckling was obtained. This investigation is in fact a severe test which demonstrates that the presented numerical procedure successfully converges with the correct solutions, even when unreasonable deflections are assumed at the beginning of the solution

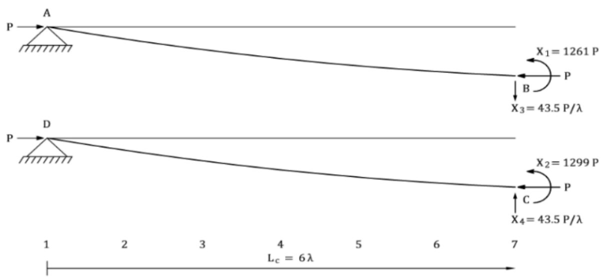

Last Cycle:

Line		1	2	3	4	5	6	7	
1-	y_{a1}	0	258	493	692	844	946	1000	
	y_{a2}	0	279	529	731	877	966	1000	
2-	M_1	0	302	580	823	1018	1164	1261	P
	M_2	0	392	738	1010	1194	1289	1299	P
3-	EIc	0.4	0.47	0.56	0.65	0.75	0.87	1.0	EI
4-	α	0	-643	-1036	-1266	-1357	-1338	-1261	P/EI
	α	0	-834	-1318	-1544	-1592	-1482	-1299	P/EI
5-	$\bar{\alpha}$		-622	-1022	-1254	-1348	-1333	-646	Pλ/EI
	$\bar{\alpha}$		-805	-1297	-1538	-1580	-1476	-683	Pλ/EI
6-	Ass. φ_{av}	6225	5603	4581	3327	1979	646		Pλ/EI
	Ass. φ_{av}	7379	6574	5277	3739	2159	683		Pλ/EI
7-	y_{1t}	0	6225	11828	16409	19736	21715	22361	$P\lambda^2$/EI
	y_{2t}	0	7379	13953	19230	22969	25128	25811	$P\lambda^2$/EI
8-	y_{1c}	0	824	1648	2472	3295	4119	4943	$P\lambda^2$/EI
	y_{2c}	0	249	498	747	995	1244	1493	$P\lambda^2$/EI
9-	y_1	0	7049	13476	18881	23031	25834	27304	$P\lambda^2$/EI
	y_1	0	7628	14451	19977	23964	26372	27304	$P\lambda^2$/EI
10-	y_{a1}/y_1		0.03660	0.03658	0.03665	0.03665	0.03662	0.03662	EI/$P\lambda^2$
	y_{a2}/y_2		0.03658	0.03661	0.03659	0.03660	0.03663	0.03662	EI/$P\lambda^2$

Better Ratio = (17230/470542) EI/$P\lambda^2$ = 0.03662 EI/$P\lambda^2$

Critical Load Pcr = 0.03662 × 36 EI/L^2c = 1.3182 EI/L^2c

Assumed Bucking Mode of Next Cycle:

y_{a1}	0	258.2	493.6	691.5	843.5	946.2	1000
y_{a2}	0	279.4	529.3	731.7	877.7	965.9	1000

Fig. 5 Calculation of critical load Pcr for multi-span sway frame of Fig. 4 (last cycle)

Table 1. Different assumed starting deflections (first cycle) all converging to the same critical load Pcr and buckling mode

	Values of Assumed Set of Deflection (1st Cycle)	Assumed shape (1st Cycle)
1	0 167 333 500 667 833 1000 Same in four columns (Straight line)	
2	0 259 500 707 866 966 1000 Same in four columns (Sine Curve)	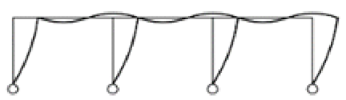
3	0 -100 0 150 450 600 1000 Same in four columns	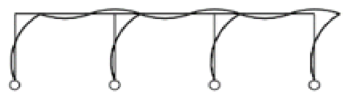
4	0 -500 -700 -700 -500 0 1000 Same in four columns	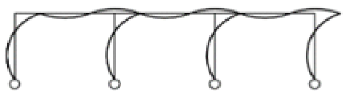
5	0 167 333 500 667 833 1000 0 259 500 707 866 966 1000 0 -100 0 150 450 600 1000 0 -500 -700 -700 -500 0 1000 Different in each column (combination of sets 1 to 4 above, unreasonable)	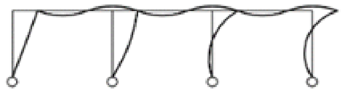

The sway critical load procedure described herein is used to calculate the buckling load for the frame shown in Fig. 6, resulting in a critical load of 5.04 EI/L_c^2. The resulting deflections (buckling modes) at seven equally spaced sections of the four columns are shown in Table 2. For example, the value of 847 for the hinged column carrying a load of 2P is the column deflection for the section whose moment of inertia is equal to 2.00 I as shown in Fig. 6. A linear set of deflection was assumed in the first cycle, resulting in a first cycle critical load of 4.97 EI/L_c^2 with a difference of just 1.4% from the final answer.

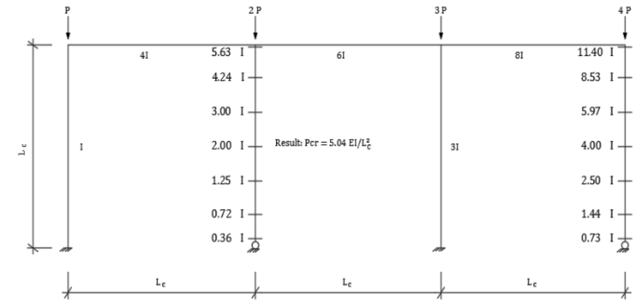

Fig. 6 Sway multi-span frame with non-prismatic members

Table 2. Buckling mode for sway multi-span frame of Fig. 5

Column	Load	Column Buckling mode values at seven sections with a top column sway Δ = 1000						
Fixed	P	0	63	230	459	698	894	1000
Hinged	2P	0	387	670	847	946	990	1000
Fixed	3P	0	65	236	469	709	902	1000
Hinged	4P	0	357	624	800	907	969	1000

The sway critical loads for multi-span frames, having 2 to 10 columns, with bending stiffness ratio K_b/K_c ranging from 0.1 to 4, are determined using the presented method. In all cases the end columns carry a load P whereas the intermediate ones are subjected to a load $2P$. The results are plotted in Figs. 7 and 8. The curves show that the value of the factor β, where $P_{cr} = \beta\, EI_c/L_c^2$, decreases as the number of columns increases. Nevertheless, the total critical load carried by the entire frame increases. The curves approach to each other more and more as nc increases, and become very close for nc greater than 6, especially for small ratios of K_b/K_c. The curves also show that the sway critical load increases with the increase of the relative bending stiffness K_b/K_c.

Since there is no difficulty in obtaining the critical loads P_{cr} of frames with nonprismatic column members using the numerical procedure described in this research, why not analyze such frames? is the critical load of such frames higher than the critical load of frames with prismatic members having equal volume? and what is the ratio of the depth at the top and bottom of the columns for maximum possible critical load? Fig. 9 shows a rectangular cross section with a constant width b and varying depth d. The dimension d_x may be expressed by

$$d_x = d_b\left[1 + \left((d_t/d_b) - 1\right)x/L\right] \qquad (10)$$

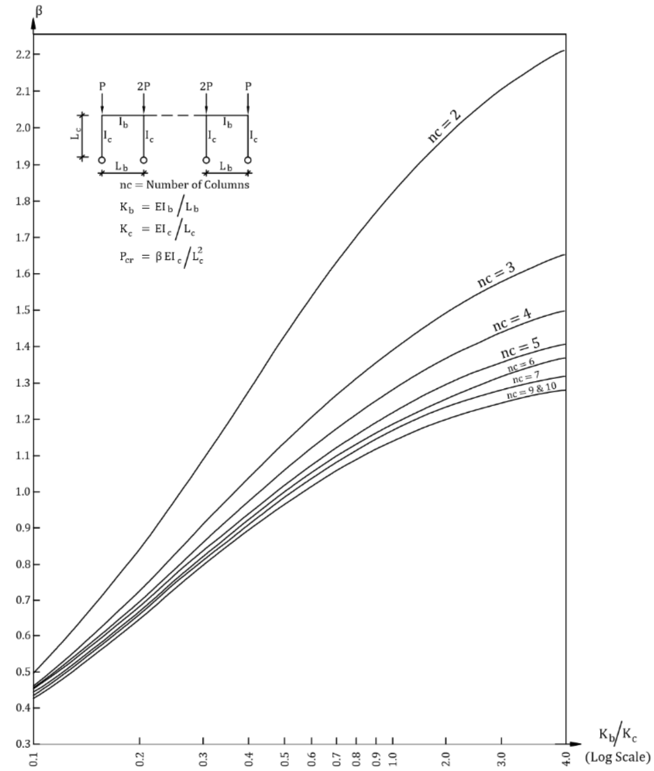

Fig. 7 Sway critical load of multi-span hinged frames

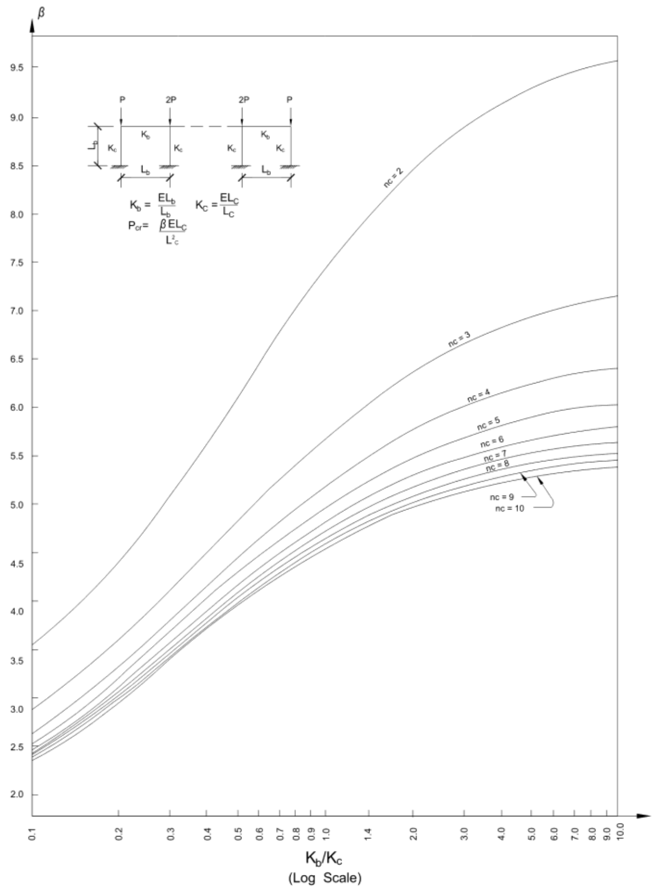

Fig. 8 Sway critical load of multi-span fixed frames

where d_x is the depth of any cross section located at distance x from bottom column's section, d_t is the depth of the top section, d_b is the depth of the bottom section and L is the height of the column. For a constant volume column having sectional depth of d_m at mid-height, where $d_m = (d_b + d_t)/2$, the moment of inertia at any section is given by

$$I_x = \left[\frac{1 + \left(\frac{d_t}{d_b} - 1\right)\frac{x}{L}}{0.5\left(\frac{d_t}{d_b} + 1\right)}\right]^3 I_m \qquad (11)$$

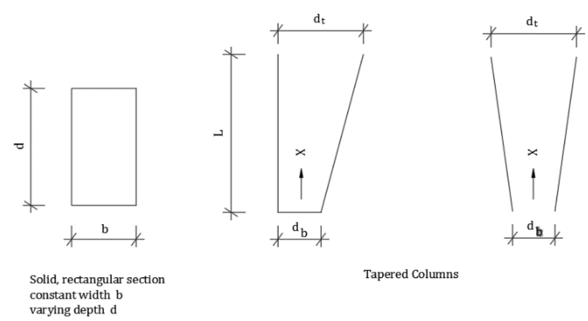

Fig. 9 Dims notation of tapered columns

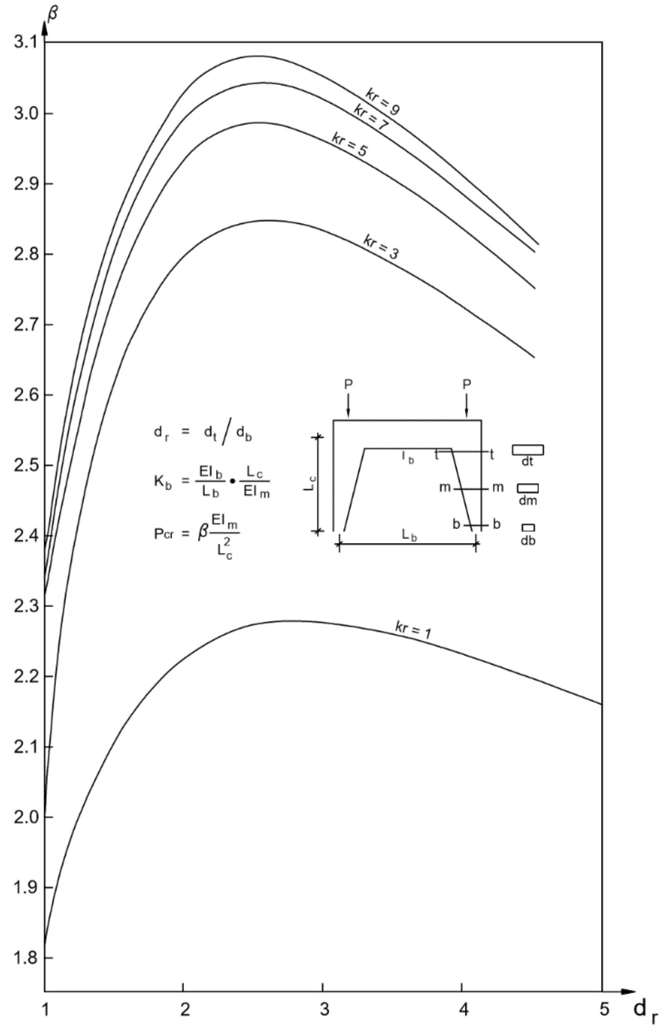

Fig. 10 Critical sway load of two hinged frames with tapered columns

where I_m is the moment of inertia at the mid-section. Using Eq. (11), the values of moment of inertia along the columns are calculated and the critical load is obtained for various ratios of d_t/d_b. The results are plotted in Figs. 10 - 12, covering the range of d_t/d_b= 1.0 to 5.0, for one, two and three spans, respectively.

Figs 10-12 present the variation of the critical sway load for one-span, two-span, and three-span hinged frames with tapered columns as a function of the depth ratio d_t/d_b where d_t and d_b are the depths at the top and bottom of the column, respectively. The analysis assumes constant column volume, and the moment of inertia at each section is computed using Eq. (11), which accounts for the variation of depth along the column height. The developed numerical procedure applies to Newmark's double integration method iteratively to determine the buckling load corresponding to each taper ratio. As shown in the figures, the critical load increases with the depth ratio up to a peak at d_t/d_b= 2.5, beyond which the load begins to decrease. This behavior reflects the trade-off between stiffness distribution and geometric efficiency: increasing the top depth improves resistance to lateral displacement, but excessive tapering reduces stiffness near the base, which is critical for buckling resistance. The maximum critical load achieved at the optimal taper ratio is approximately 25–30% higher than that of a prismatic column with the same volume. These results confirm that strategic tapering can significantly enhance the buckling performance of multi-span frames, especially in systems with hinged support where lateral stability is more sensitive to column geometry.

The effective length factor k is given by $k = \pi/\sqrt{\beta}$ where the critical load, P_{cr} can be determined using $P_{cr} = \frac{\pi^2 EI_m}{(kL_c)^2}$

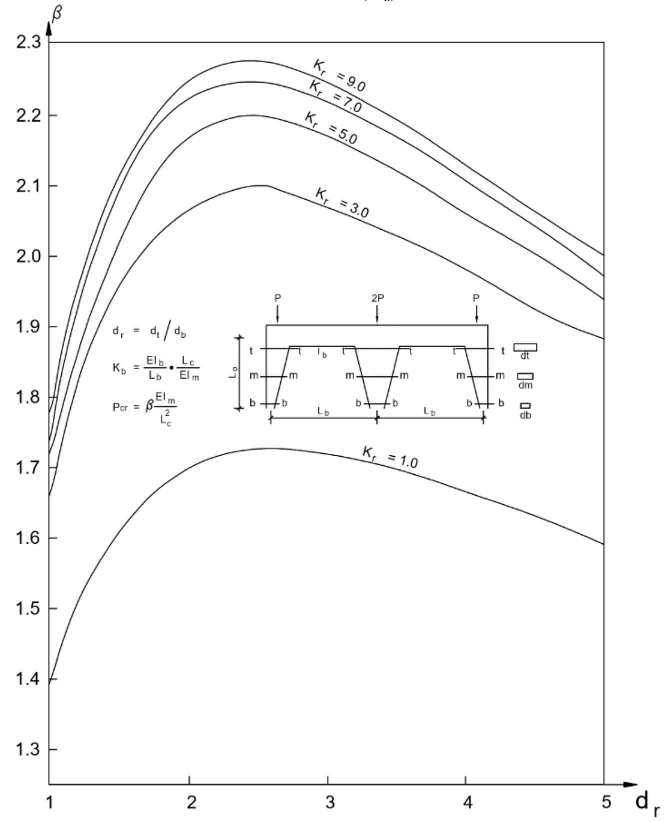

Fig. 11 Critical sway load of two span hinged frames with tapered columns

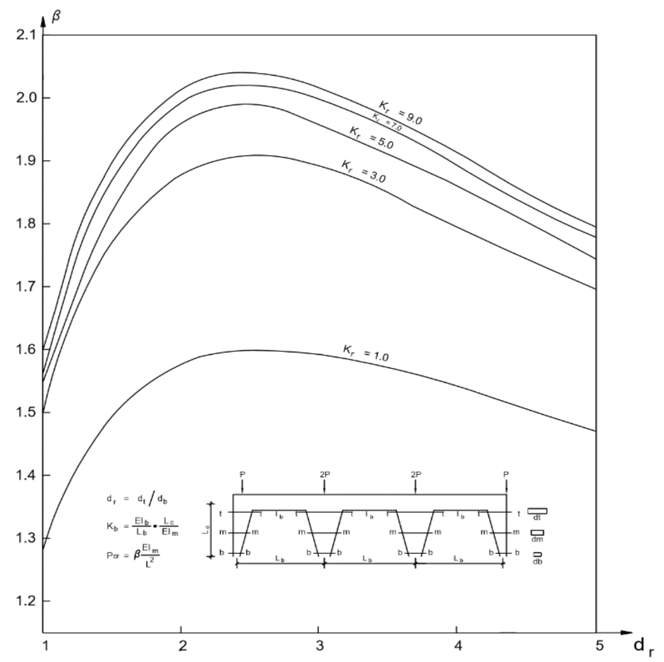

Fig. 12 Critical sway load of three span hinged frames with tapered columns.

4. Conclusions

The following key findings are drawn from this study (1) Newmark's numerical double integration method was successfully extended for use in computing critical loads and buckling modes of rigidly jointed sway elastic multi-span portal frames with mixed hinged and fixed columns, (2) the method accurately computes critical buckling loads and effective length factors for prismatic and non-prismatic columns, (3) the elastic line of the mode of buckling is determined as a major part of the solution, which gives a clear insight of the behavior of the structure, (4) a depth ratio of 2.5 between the top and bottom of tapered columns yields the maximum critical load, (5) tapered columns with constant volume can achieve 25–30% higher critical loads than prismatic columns, (6) the method converges reliably even with arbitrary initial deflection assumptions, demonstrating robustness, (7) the method can be used to calculate the column effective length factor and the buckling loads of frames with non-prismatic members having irregular shapes, and (8) the approach is applicable to steel and concrete frames in buildings, bridges, and industrial structures.

Funding

This research did not receive any specific grant from funding agencies in the public, commercial, or not-for-profit sectors.

References

ACI 318 (2025), Building code requirements for structural concrete and commentary, American Concrete Institute; Farmington Hills, MI, USA.

AISC (2023), Steel Construction Manual 16th ed., American Institute of Steel Construction, USA.

Badir, A. (2011), "Elastic buckling loads of hinged frames by the Newmark method," International Journal of Applied Sciences and Technology, 1(3), 14-21.

Badir, A. (2020), "Elastic buckling loads of fixed frames by the Newmark method," Electronic Journal of Structural Engineering, 20(1), 1-5. https://doi.org/10.56748/ejse.20239

Bazeos, N. and Karabalis D. "Efficient Computation of buckling loads for plane steel frames with tapered members," Engineering Structures 28, 771-775. https://doi.org/10.1016/j.engstruct.2005.10.004

Behjati-Avval, M. and Kalatjari, V. (2015) "Determination of the effective length factor for non-prismatic columns in two-span gable frames," Current World Environment, 10(special issue 1), 421-428, https://doi.org/10.12944/CWE.10.Special-Issue1.53

Belabed, Z., Tounsi, A., Bousahla, A.A. and Yaylacı, M. (2024) "Accurate free and forced vibration behavior prediction of functionally graded sandwich beams with variable cross-section: A finite element assessment," Mechanics Based Design of Structures and Machines, 52(11), 9144-9177. https://doi.org/10.1080/15397734.2024.2337914

Belabed, Z., Bousahla, A.A. and Tounsi, A. (2024), "Vibrational and elastic stability responses of functionally graded carbon nanotube reinforced nanocomposite beams via a new Quasi-3D finite element model," Computers and Concrete, 34(5), 625-648. https://doi.org/10.12989/cac.2024.34.5.625

Belabed, Z., Tounsi, A., Bousahla, A.A., Khedher, K.M., Salem and M.A. (2024), "Mechanical behavior analysis of FG-CNTRC porous beams resting on Winkler and Pasternak elastic foundations: A finite element approach," Computers and Concrete, 34(4), 447-476. https://doi.org/10.12989/cac.2024.34.4.447

Belabed, Z., Tounsi, A., Bousahla, A.A., Bourada, M. and Al-Osta, M.A. (2024) "Free vibration analysis of Bi-Directional Functionally Graded Beams using a simple and efficient finite element model," Structural Engineering and Mechanics, 90(3), 233-252. https://doi.org/10.12989/sem.2024.90.3.233

Belabed, Z., Tounsi, A., Al-Osta, M.A. and Minh, H.L. (2024) "On the elastic stability and free vibration responses of functionally graded porous beams resting on Winkler-Pasternak foundations via finite element computation," Geomechanics and Engineering, 36(2), 183-204. https://doi.org/10.12989/gae.2024.36.2.183

Bentrar, H., Chorfi, S.M., Belalia, S.A., Tounsi, A., Ghazwani, M.H. and Alnujaie, A. (2023), "Effect of porosity distribution on free vibration of functionally graded sandwich plate using the P-version of the finite element method," Structural Engineering and Mechanics, 88(6), 551-567. https://DOI: 10.12989/sem.2023.88.6.551

Bradford, M. A. and Abdoli Yazdi, N. (1999) " A Newmark-based method for the stability of columns," Computers & Structures, 71, 689-700. https://doi.org/10.1016/S0045-7949(98)00219-3

BSI (2005) Design of steel structures general rules for buildings, London 1993-1

Duan L and Chen WF (1988) "Effective length factor for columns in braced frames," Journal of Structural Engineering, ASCE 114(10), 2357-2370. https://doi.org/10.1061/(ASCE)07339445(1988)114:10(2357)

Duan L and Chen WF (1989) Effective length factor for columns in unbraced frames. Journal of Structural Engineering: ASCE 115(l): 149-165. https://doi.org/10.1061/(ASCE)0733-445(1989)115:1(149)

Duan, L. and Chen, W.F. (1999) "Effective Length Factors of Compression Members" Structural Engineering Handbook Ed. Chen Wai-Fah Boca Raton: CRC Press LLC, 1999

Euler, L (1778), "Determinatio onerum, quae columnae gestare valent," Acta Academiae Scientiarum Petropolitanae 1(a), 121-145 (in Latin).

Godoy, L.A. and Elishakoff, I. (2020), "The experimental contribution of Petrus Van Musschenbroek to the discovery of a buckling formula in the early 18th century", International Journal of Structural Stability and Dynamics, 20(5), 1-28. https://doi.org/10.1142/S0219455420500637

Julian, O.G. and Lawrence, L.S. (1959), Notes on J and L nomographs for determination of effective lengths (unpublished report).

Katiyar, V., Gupta, A. and Tounsi, A. (2022) "Microstructural/geometric imperfection sensitivity on the vibration response of geometrically discontinuous bi-directional functionally graded plates (2D-FGPs) with partial supports by using FEM," Steel and Composite Structures, 45(5), 621-640.

Kishi N., Chen W.F. and Goto, Y. (1997) "Effective length factor of columns in semi-rigid and unbraced frames," Journal of Structural Engineering: ASCE 123(3): 313-320. https://doi.org/10.1061/(ASCE)0733-9445(1997)123:3(313)

Krynicki, E.J. and Mazurkiewicz, Z.E. (1964), "Frames of solid bars of varying cross sections," J. Struct. Div., ASCE, 90(ST4), 145-174. https://doi.org/10.1061/JSDEAG.0001115

Lakhdar, Z., Chorfi, S.M., Belalia, S.A., Khedher, K.M., Alluqmani, A.E., Tounsi, A. and Yaylacı, M. (2024) "Free vibration and bending analysis of porous bi-directional FGM sandwich shell using a TSDT p-version finite element method,". Acta Mechanica, 235, 3657-3686. https://doi.org/10.1007/s00707-024-03909-y

Lee, B. K. and Lee, J. K (2021) "Buckling of Tapered Heavy Columns with Constant Volume," Mathematics, 9(6), 657. https://doi.org/10.3390/math9060657

Li, Q., Zou, A. and Zhang, H. (2016), "A simplified method for stability analysis of multi-story frames considering vertical interactions between stories." Advances in Structural Engineering, 19(4), 599-610. https://doi.org/10.1177/1369433216630191

Musschenbroek, P. (1729) Physicæ experimentales, et geometricæ, de magnete, tuborum capillarium vitreorumque speculorum attractione, magnitudine térrea, cohaerentia corporum firmorum. Dissertationes, ut et Ephemerides meteorologicae Ultrajectinae, Lugdun Batavonum, apud Samuelem Luchtmans, (in Latin). https://doi.org/10.1163/9789004579835

Naidoo, D. and Li, K. (2019), "Optimization of no sway plane rigid frames against buckling," Journal of Civil Engineering Research, 9(1), 1-15.

Newmark, N.M. (1943), "Numerical procedure for computing deflections, moments, and buckling loads," Trans. ASCE. 108,1161-1943. https://doi.org/10.1061/TACEAT.0005640

Nikolić, A. and Šalinić, S. (2017), "Buckling Analysis of non-prismatic columns: A rigid multibody approach," Engineering Structures, 143, 511-521. https://doi.org/10.1016/j.engstruct.2017.04.033

Oppe, M., Muller, C., and Iles, C. (2005) NCCI: buckling lengths of columns; rigorous approach. London: Access Steel.

Pomares JC, Pereiro-Barceló J, González A, Aguilar R. Safety Issues in Buckling of Steel Structures by Improving Accuracy of Historical Methods. Int J Environ Res Public Health. 2021 Nov 22;18(22):12253. PMID: 34832006; PMCID: PMC8618944. https://doi.org/10.3390/ijerph182212253

Rayhan, S. B., Rahman, M. M., Sultana, J., Szávai, S., & Varga, G. (2025), "Finite Element and Machine Learning-Based Prediction of Buckling Strength in Additively Manufactured Lattice Stiffened Panels," Metals, 15(1), 81. https://doi.org/10.3390/met15010081

Rezaiee-Panjad, M., Shahabian, F. and Bambaeechee, M. (2016), "Stability of non-prismatic frames with flexible connections and elastic supports," KSCE Journal of Civil Engineering, 20(2), 832-846. https://doi.org/10.1007/s12205-015-0765-6

Schilling, Charles G. (1983). "Buckling of One-Story Frames," Engineering Journal, American Institute of Steel Construction, Vol. 20, pp. 49-57. https://doi.org/10.62913/engj.v20i2.395

Tati, A. (2021), "Finite Element Analysis of thermal and mechanical buckling behavior of functionally graded plates," Archive of Applied Mechanics, vol. 91, pp. 4571-4587 https://doi.org/10.1007/s00419-021-02025-w

Tian, W., Hao, J. and Zhong, W (2021a) "Buckling of stepped columns considering the interaction effect among columns", Journal of construction steel research, 177 https://doi.org/10.1016/j.jcsr.2020.106416

Tian, W., Sun, J, and Hao, J. (2021b) "Effective length factors of three- and two-segment stepped columns", Journal of construction steel research, 181 https://doi.org/10.1016/j.jcsr.2021.106585

Timoshenko, S.P. and Gere, J.M. (1964) Theory of Elastic Stability, (2nd ed.) McGraw-Hill, New York, NY, USA.

Tounsi, A., Belabed, Z., Bounouara, F., Balubaid, M., Mahmoud, S.R., Bousahla, A.A., and Tounsi, A. (2024), "A finite element approach for forced dynamical responses of porous FG nanocomposite beams resting on viscoelastic foundations," https://doi.org/10.1142/S0219455426500781

International Journal of Structural Stability and Dynamics, Online Ready. https://doi.org/10.1142/S0219455426500781

Weber, A., Orr, J.J., Shepherd, P. and Crothers, K. (2015) "The effective length of columns in multi-storey frames", Engineering Structures, 102, 132-143. https://doi.org/10.1016/j.engstruct.2015.07.039

Disclaimer